HHS Public Access

Author manuscript

Small. Author manuscript; available in PMC 2017 May 01.

Published in final edited form as:

Small. 2016 May ; 12(19): 2616–2626. doi:10.1002/smll.201503342.

Controlled Drug Release and Chemotherapy Response in a Novel Acoustofluidic 3D Tumor Platform

Dr. Ioannis K. Zervantonakis and

Department of Cell Biology, Harvard Medical School, 240 Longwood Ave, C1/501, Boston, 02115, MA

Dr. Costas D. Arvanitis

Department of Radiology, Harvard Medical School, Brigham and Women's Hospital 221 Longwood Ave, 514a, Boston, 02115, MA

Costas D. Arvanitis: cda@bwh.harvard.edu

Abstract

Overcoming transport barriers to delivery of therapeutic agents in tumors remains a major challenge. Focused ultrasound (FUS), in combination with modern nanomedicine drug formulations, offers the ability to maximize drug transport to tumor tissue while minimizing toxicity to normal tissue. This potential remains unfulfilled due to the limitations of current approaches in accurately assessing and quantifying how FUS modulates drug transport in solid tumors. We developed a novel acoustofluidic platform by integrating a physiologically relevant 3D microfluidic device and a FUS system with a closed-loop controller to study drug transport and assess the response of cancer cells to chemotherapy in real time using live cell microscopy. FUS-induced heating triggered local release of the chemotherapeutic agent doxorubicin from a liposomal carrier and resulted in higher cellular drug uptake in the FUS focal region. This differential drug uptake induced locally confined DNA damage and glioblastoma tumor cell death in the 3D environment. Our study demonstrates the capabilities of acoustofluidics for accurate control of drug release and monitoring of localized cell response in a 3D *in vitro* tumor model and has important implications for developing novel strategies to deliver therapeutic agents directly to the tumor tissue while sparing healthy tissue.

Graphical Abstract

A novel 3D acoustofluidic tumor platform to study the effects of focused ultrasound-triggered drug release in glioma cell lines in real time and monitor tumor cell death and DNA damage. This platform can be used to discover new non-invasive protocols that target tumor cells regionally without damaging normal cells.

Correspondence to: Costas D. Arvanitis, cda@bwh.harvard.edu.

Supporting Information

Supporting Information is available from the Wiley Online Library.

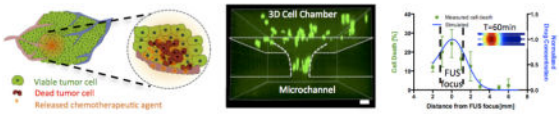

Keywords

acoustofluidics; 3D tumor model; focused ultrasound; controlled release; tumor microenvironment

1. Introduction

Solid tumors constitute a complex transport milieu that hinders the effective delivery of potent therapeutics [1]. The high interstitial fluid pressure and the chaotic and tortuous vascularization that characterize solid tumors, limit the extravasation and penetration of drugs to the tumor core [2]. Dose escalation to improve drug accumulation and penetration in the tumor core is prohibitive due to adverse systemic effects associated with nonspecific delivery [3]. To overcome these obstacles, novel nanoparticle drug formulations have been developed that have increased tumor accumulation and are associated with lower toxicity and clearance times [4]. Despite initial promising results of these nanoparticle-based therapies, their efficacy remains limited and novel approaches are required to improve their therapeutic index [5].

Technologies employing methods of local drug release hold great promise for the development of effective and safe anticancer treatment protocols that deliver therapeutic agents directly to the tumor tissue without damaging healthy tissue [6]. Focused ultrasound (FUS), that delivers acoustic energy in a small focal region, typically a few millimeters (mm) wide, has been used to not only modulate the permeability of tumor vessels and enhance the extravasation of large molecules [7] but to also locally trigger the release of their highly penetrating cargo [8, 9]. Although recent animal studies have demonstrated that FUS-triggered release and delivery of chemotherapeutic agents can induce tumor regression in xenografts [10, 11], the clinical translation of this technology requires further improvements in protocol parameters, drug distribution and treatment-associated toxicities [12].

Physiologically relevant 3D tumor *in vitro* models could greatly aid in designing nanoparticle-based treatment protocols and understanding the cellular and molecular mechanisms involved [13]. These *in vitro* models can be utilized early in the drug discovery process to optimize the therapeutic index of these protocols in order to achieve a balance between sufficient drug exposure to induce cytotoxic effects to tumor tissue, while sparing normal cells [14].

Microfluidic technology provides an experimental platform where cellular environments can be accurately controlled [15] in order to model and study the effects of multiple parameters of the complex tumor transport milieu on cell behavior (e.g. 3D matrices [16], interstitial flow [17], interactions with endothelial cells [18], lymphocytes [19] and macrophages [20], hypoxia [21], nanoparticle diffusion [22], etc.). In addition, microfluidic systems that incorporate 3D tumor cell cultures [23] have been designed to study the role of cytotoxic

therapies on tumor cell response and to recreate specific organ environments [24]. Despite the development of a number of microfluidic devices coupled with ultrasound instrumentation (acoustofluidics) for particle [25, 26] and cell manipulation [27, 28] and cell-cell interactions studies [29, 30], there is no physiologically relevant 3D culture system to date, that can be used to study the effects of FUS-triggered drug release and delivery on cancer cell behavior.

In order to address the need for a model to study the underlying transport and biological mechanisms involved in localized drug release, we developed a novel acoustofluidic 3D tumor platform that is composed of an optically transparent microfluidic device (chip) and a FUS system with a closed-loop controller. The design and integration of these components results in a physiologically relevant *in vitro* model that provides a simple, tightly controlled environment that can be used to investigate the release and transport of drugs, while monitoring, in real time, the response of tumor cells in a 3D configuration. We use this acoustofluidic model to locally activate by FUS-induced heating, temperature-sensitive liposomal doxorubicin and study on-chip its release profile and chemotherapeutic efficacy on a glioblastoma cell line. By controlling the FUS excitation frequency we are able to control the size of the drug release area and induce tumor cell drug uptake, DNA damage and death in a confined area. Our results demonstrate the utility of this experimental platform for accurately controlling the location and timing of drug release in a 3D *in vitro* tumor model while studying cell response in real time. These studies of localized drug release and cell response have important implications for developing optimized FUS-based therapeutic protocols to locally target tumor cells while sparing normal cells.

2. Results

2.1 Design and Fabrication of the Acoustofluidic Platform

We developed an acoustofluidic platform that is composed of a multilayer microfluidic device with a closed loop FUS system in order to accurately control the location and area of FUS-triggered drug-release in a 3D tumor model (dashed circle, Figure 1A) and study tumor cell death in response to chemotherapy (red cells, Figure 1A). The microfluidic device included four layers that were vertically integrated (Figure 1B) for the FUS transducer to deliver pressure waves perpendicularly. This vertical integration was one of the critical aspects of this design, as it allowed for the FUS-triggered thermal and mechanical effects to be localized at the interface between the microchannel mimicking a blood-vessel (blue layer, Figure 1B) and the collagen-filled cell culture chamber (red layer, Figure 1B). The cell culture chamber dimensions (2×8 mm) were selected to allow for multiple simultaneous observations.

The separation of the cell culture chamber and the microchannel was achieved by optimizing the process of pore formation in the glass coverslip, so that we could prevent the cell-collagen gel mixture from spilling over to the DST microchannel. By varying the laser-power, we were able to change the size of the pores formed in the glass coverslip; we found the optimal area of the pore to be 0.01 mm^2 (suppl. methods and Figure S1). After the cell-collagen gel mixture was loaded in the cell culture chamber and the crosslinking of the collagen was completed, the tumor cells were confined in the cell chamber. Following the collagen croslinking, endothelial cells were seeded in the microchannel and formed a vessel

mimicing monolayer (magenta staining, Figure 1B). Finally the microfluidic device was integrated to a clossed-loop FUS system (Figure 1C).

2.2 Experimental and Numerical Characterization of FUS Physics and Drug Transport in the Microfluidic Device

We used a hydrophone and a thermochromic film to measure the pressure and temperature fields of the FUS focal region (Figure 2A) at two FUS operating frequencies. At the fundamental frequency (1.025 MHz) the full width at half maxima (FWHM) was 9 mm and 1.7 mm in the axial and transverse directions respectively (blue curve, left panel Figure 2B). The heated region was constrained in the same area with a 3.5 mm radius (green curve, left panel Figure 2B). When the transducer was operated at the 3rd harmonic frequency (3.525 MHz), the FWHM was 3 mm and 0.5 mm in the axial and transverse directions respectively (blue curve, right panel Figure 2B). At this frequency the temperature profile was confined within a radius of 1 mm (Figure 2B). These results demonstrate the ability to control the extent of the heated region (fraction or whole) within the cell culture chamber by modulating the FUS operating frequency (Movie S1 and Figure S2).

To confirm that the FUS energy can be delivered reproducibly to the microfluidic device we incorporated a temperature sensor to monitor in real time the FUS-induced temperature rise. We also integrated a pressure sensor to record microbubble oscillations from ultrasound contrast agent microbubbles flowing in the channel. These real-time measurements can be fed into a computer-based controller to fine-tune the amplitude of the FUS waves in order to accurately control these effects in the microfluidic device (Figure 2C). Figure 2D shows the ability of the controller to maintain constant temperature (37.7 °C) in the microfluidic device with a sharp rise time (7 sec) and a narrow temperature range (±0.1 °C). The pressure sensor, operated in passive mode, was also able to detect harmonic and ultra-harmonic emissions from sonicated microbubbles that were flowing in the flow microchannel (Figure 2E).

We developed a computational transport model to characterize diffusion in the acoustofluidic device and evaluate the region where free doxorubicin could diffuse after FUS-triggered release (Figure 2F). First, we validated this computational model by comparing the simulated concentration profiles with measurements of a fluorescent tracer with a similar molecular weight to the chemotherapeutic agent doxorubicin. The simulated temporal and spatial concentration profiles (Figure 2G, H) agreed well with the experimental data. To model doxorubicin diffusion after FUS-triggered release from the liposomes, we used the measured temperature profile (Figure 2A, fundamental frequency) as input for the initial distribution of free doxorubicin. These simulations show that free doxorubicin had diffused across all regions of the cell culture chamber 60min after FUS-triggered drug release.

2.3 Controlled Release and Cell Response to Liposome-Encapsulated Chemotherapy

To demonstrate the potential of our integrated platform to study FUS-based therapeutic protocols we assessed its ability to activate doxorubicin-loaded heat-sensitive liposomes and study on-chip the cellular response of cancer cells to the released drug. We selected doxorubicin because preclinical data demonstrate that it is toxic to glioblastoma cell

lines [31] and it is a chemotherapy compatible with nanoparticle formulations used in the clinic for multiple solid tumors [32].

We used the highly aggressive F98 rat glioblastoma cell line [33] that we engineered to express GFP in order to follow cell response in the same group of cells over time. Next, we characterized the dose response of the glioblastoma cells to the doxorubicin-TS-liposomes utilizing a 2D scanning cytometer assay to identify a drug concentration at which cytotoxicity would be differentially affected by heat-induced release. We found the concentration of 0.3 μM as an optimal dose where the difference in viable cell numbers between heat-triggered drug release and no release was maximal (black line, Figure 3A). Furthermore, at this dose we observed a significant increase in cell death compared to the no release control (Figure 3B). We selected this dose of 0.3 μM for our follow-up experiments in the acoustofluidic device in order to study cell responses at a concentration with a good therapeutic index (large difference between the heat-induced drug-release compared to no release).

We then evaluated the response of the F98 cells in the microfluidic device under 3D culture conditions, where the glioblastoma cells where embedded in a collagen hydrogel (Figure 3C). These experiments were performed in the absence of an endothelial monolayer, since endothelial cells did not alter tumor cell viability after treatment with doxorubicin-TS-liposomes (Figure S3). Under control conditions, with no drug-treatment, we observed a high level of tumor cell proliferation with an increase of 258.1 ± 50.6 % in cell numbers and a low baseline level of cell death with 9.5 ± 1.5 % of dead cells over total cells at 48hrs (Figure 3D–E). Compared to control conditions, treatment of the glioblastoma cells with 0.3 μM of encapsulated doxorubicin resulted in reduced tumor cell proliferation (41.1 ± 15.8%, p=0.03) but only had a mild effect in cell death (12.4 ± 1.8%, p=0.57). Importantly, under heat-induced drug release using a water bath, we observed a significant increase in cell death (34.5 ± 12.3 %, p=0.02) and a reduction in tumor cell numbers (−11.7 ± 25.3% p=0.04). Under conditions of FUS-triggered release (fundamental frequency at 2.7 Watts acoustic power with heating for 12 minutes: Figure S2A; doxorubicin distribution: Figure 2F) we observed a similar reduction in tumor cell numbers (−21.3 ± 16.0 % p=0.02) and an increase in cell death (33.2 ± 6.3 % p=0.001). To assess the potential effects of FUS-triggered heating on cell behavior, we also analyzed devices where no drug was added and found that the FUS-treatment did not alter tumor cell death (8.2 ± 1.2%, p=0.54) but slowed tumor cell proliferation (158.8 ± 55.1%, p=0.17) compared to the control devices. Exposure of the devices to heating at 43 °C using a water bath had similar effects with a small reduction in proliferation (205.3% ± 80.6%, p=0.49) and no effects on cell death (8.4 ± 1.4%, p=0.62). The effects of heating on cell proliferation and death were also confirmed using well-plate experiments (Figure S4). In all experiments the measured thermal dose (15–18 equivalent minutes at 43 °C) was just below the threshold value of 17–20 equivalent minutes for irreversible cell damage [34, 35]. These results are in agreement with the measurements in the 2D well plate and demonstrate that FUS-controlled drug release within our acoustofluidic device can be used to study cytotoxic effects of chemotherapy.

We further investigated the effects of FUS-triggered doxorubicin release on the expression of a DNA damage marker by performing immunostaining in the microfluidic device. In

particular, we used immunofluorescence-based quantification of phosphorylated histone H2AX (γ-H2AX), which is a sensitive and reliable marker of DNA damage [36]. Under conditions of FUS-triggered drug-release we observed multiple distinct bright foci in the nuclei (Figure 4A bottom row versus other two rows) indicating that the released doxorubicin induces DNA damage. Quantification of these images showed a significant increase in H2AX phosphorylation under FUS-triggered drug release compared to both drug treatment without heating (2.4 ± 0.3 fold change, p=0.0002) and FUS heating only (2.6 ± 0.4 fold change, p<0.0001) (Figure 4B). These immunofluorescence data together with the cell viability measurements demonstrate that FUS-triggered doxorubicin release induced DNA-damage followed by tumor cell growth inhibition and cell death.

2.4 Localized Drug Release and Response to Drug Gradients

A very important feature of the design presented here is the ability to control the size of the heated area and the resulting drug diffusion radius by tuning the FUS operating frequency. We hypothesized that under localized drug release conditions we could induce tumor cell death in a spatially confined region, while keeping tumor cells intact in the remaining part of the cell culture chamber.

By using the third harmonic (3.525 MHz, 2.2 Watts acoustic power) of the FUS transducer and setting the temperature controller at 43.5 °C we confined the heated region (at a temperature greater than 41 °C) to a circular area of 2 mm in diameter (right panel, Figure 2B). Computer simulations of drug diffusion in the device were performed to evaluate the extent to which the drug would diffuse after localized release (Figure 5A, B). These simulations were supported by doxorubicin uptake measurements that confirmed the significantly higher doxorubicin uptake in the region of release (R) versus the region of no release (NR, 3-fold difference, p<0.0001, Figure 5C). In addition, to investigate the stability of FUS-triggered release we measured the temperature temporal profile that exhibited minimal variation (43.5 ± 0.3 °C, Figure S2B).

To assess the effects of localized drug release on cell response we measured tumor cell death as a function of the distance from the center of the FUS focus. We found that the percentage of dead tumor cells reached a maximum value of 40.9 ± 7.4 % at the center of the FUS focus (x=0mm) and decayed to a baseline value of 18.8 ± 3.4 % towards the edges (x=6mm) of the cell chamber (baseline-corrected cell death profile plotted in Figure 5B, black bars). Interestingly, the distribution of these cell death measurements agreed very well with the simulated drug concentration profile, where high drug concentrations (50% of maximum dose 0.3μM) were expected in a region with a radius of 2 mm (Figure 5B). Validation experiments confirmed that these differential effects on cell death were due to drug release, since there was no significant trend in cell death levels across the device for the condition of FUS treatment only (Figure 5B, grey bars, p=0.14 for comparing cell death at x=0mm versus x=6mm). The level of cell death measured in this confined region of drug release is consistent with measurements in the experiments where the FUS focus spanned across most of the cell chamber (Figure 3E). Importantly we observed differences in cell proliferation (Figure S5B) that were consistent with the global doxorubicin release experiment (Figure 3C) and compared DNA damage markers (Figure 5D and Figure S5A) between a region that

was at the focus of the FUS (x=0mm) with a region that was further away (x=6mm). Specifically, compared to the control untreated devices (no FUS and no drug), a significant increase in expression of phosphorylated H2AX was found in the region (x=0mm, R) of drug-release (2.5 ± 0.3 fold change, $p<0.0001$) versus no differences at the region (x=6mm, NR) of no-release (1.1 ± 0.1 fold change, $p=0.87$).

Finally we monitored tumor cell fate in response to doxorubicin release and demonstrated in real-time the induction of increased cell death in an area of drug release (Figure 6A, Movie S3, 4) compared to an area of no doxorubicin release. Quantification of tumor cell death (Figure 6B) in these live cell imaging experiments confirmed the differential effects of cell death that we found using end-point measurements (Figure 5B). Collectively, these findings demonstrate that by controlling the underlying drug release conditions, cell phenotypic responses and associated cellular mechanisms at the protein level can be induced locally and monitored within the acoustofluidic chip.

3. Discussion

Experimental models that allow for the systematic investigation of drug delivery barriers (e.g. interstitial fluid pressure, blood-brain-barrier, etc.) are essential for the development of optimal nanomedicine-based treatment strategies [1]. We presented a new acoustofluidic system composed of a 3D microfluidic tumor model with a FUS system that includes a closed-loop controller, and demonstrated its utility in studying localized drug release and cell response to chemotherapy in a physiologically relevant microenvironment. This integration enables the use of FUS to trigger the release of anticancer agents from heat-sensitive nanocarriers, thereby allowing for increased control over drug delivery. We demonstrated that localized drug release of doxorubicin resulted in locally confined DNA damage and tumor cell death in a 3D collagen gel (Figure 5).

By tuning the FUS frequency we induced mild hyperthermia and chemotherapeutic agent release from thermally sensitive liposomes in a confined region. We measured cell viability in response to various doxorubicin doses (Figure 3) and also used immunofluorescence staining (Figure 4) to investigate DNA damage response at the protein level. The differences in cell viability between heating- or FUS-triggered release (43 °C) and no release (37 °C) are in agreement with the reported change in the drug release rate of these thermally sensitive liposomes at these temperatures[37]. In addition, the observed doxorubicin-induced phosphorylation of H2AX, as distinct bright foci in the nuclei (Figure 4A), suggests that low doses of doxorubicin can induce DNA damage in this glioblastoma cell line. This is further supported by the higher levels of γ-H2AX staining with increasing doses of doxorubicin-TS-liposomes (Figure S6). Our cell viability measurements are comparable with published results of doxorubicin doses (~0.2 μg/mL) that reduce F98 viability to 50% [38]. Furthermore, the differences in cell viability between no-doxorubicin release and heat-induced release are consistent with a recent *in vitro* cytotoxicity study using similar heat-sensitive doxorubicin loaded liposomes in murine melanoma and human pancreatic cell lines [39].

Our 3D model provides control over a range of important parameters in the tumor microenvironment. First, it allows for the establishment of either convection-dominated or diffusion-dominated transport by controlling the flow parameters in the DST microchannel (Movie S2). Second, it makes it possible to investigate drug transport phenomena and tumor cell death in a more complex tumor microenvironment by incorporating an endothelial monolayer [20] in the vertical flow-channel (Figure 1B) or stromal cells (e.g. astrocytes) directly adjacent to the tumor cells in the cell culture chamber. In addition, it provides the flexibility of the FUS technology, where different settings of piezoelectric crystal geometry, frequency and power can be used to fine-tune the size of the targeted region and the applied thermal and mechanical forces on tissues. FUS is also an attractive technology for translation into the clinic [40]. Hence, our acoustofluidic platform could be a useful tool for investigating anticancer therapies that aim to maximize the therapeutic index by delivering high concentrations at the tumor core while minimizing exposure to adjacent healthy tissue (e.g. infiltrative brain tumors [2]).

The technology integration that we present here offers significant advantages over existing ultrasound-based *in vitro* systems. Previous designs that were compatible with FUS and incorporated 3D culture chambers with flow-channel, lacked control of the transport phenomena (i.e. no concentration gradients could be established) [41] and did not incorporate any real-time drug release control mechanisms [42, 43]. In addition, other device designs that incorporated fluid flow control did not employ 3D cell culture and did not allow modulation of the FUS parameters [44]. Moreover, the vertical design allows for a direct visualization of the effects of FUS induced acoustic cavitation on cells. For example, the acoustic waves could push the microbubbles in this flow channel towards the free interface to interact with cells, competing against pressure gradients or other modelled biological barriers. Finally, the integration of a closed loop controller allows for reproducible delivery of acoustic waves to the flow channel and the cells in the culture chamber.

Currently available tumor models are not adequate for simultaneously studying tumor cell response and transport mechanisms under spatial and temporal control of the drug release location. The acoustofluidic platform presented here however, overcomes these barriers. It can be used to simulate different transport regimes by controlling for the fluid flow and drug concentrations in the cell culture chamber, and the modular design allows for incorporation of key characteristics of the complex solid tumor microenvironment. Furthermore, due to the small volume of the reagents required for experimental operation, the developed platform could be used as a test-bed for drug development with FUS compatible nanocarriers.

4. Conclusion

Transport barriers in drug delivery represent an ongoing challenge in cancer treatment. While nano-medicine-based anticancer therapies show some promise in overcoming these barriers and decreasing toxicity associated with nonspecific delivery, further treatment protocol optimization is necessary. One of the challenges with the development of localized therapies is the establishment of physiologically relevant assays that model critical features of the tumor microenvironment and allow for a systematic investigation of drug delivery methods and the resulting cellular response mechanisms. To address this need, we developed

a new acoustofluidic device with integrated sensors and FUS transducer, and a framework to quantify the effects of localized drug release on tumor cell response in real time. We demonstrated control of the size of the drug release area by tuning the operating frequency of the transducer and characterized drug transport both experimentally and computationally. Using this system, we were able to locally release doxorubicin and provided new evidence that cellular drug uptake, DNA damage and tumor cell death were confined to the area of drug release. Our acoustofluidic platform can be used for the discovery of new therapeutic protocols for non-invasive cancer treatments that target tumor cells regionally without damaging adjacent normal cells.

5. Experimental Section

Microfluidic Device

The microfluidic device design includes four components: i) the cell culture chamber, ii) the glass coverslip with etched pores, iii) the flow channel, and iv) the glass coverslip. The cell culture chamber was fabricated following soft photolithography procedures using Polydimethylsiloxane (PDMS). The rectangular flow channel (width: 2.5 mm; height: 170 μm) was made out of double sided tape (DST) (Adhesives Research, Glen Rock, PA, USA) using a laser cutter (VLS 3.50, Universal Laser Systems, Scottsdale, AZ, USA). This DST flow layer was bonded on a glass coverslip to form the flow microchannel. To enable transport between the DST flow channel and the PDMS cell chamber, eight pores were etched in a glass coverslip (size: 22×40 mm, thickness: 130 μm) using the laser cutter. The area of the pores was optimized to restrict the collagen-cell mixture within the cell chamber (Figure S1 and suppl. methods). All the components were autoclaved before the vertical assembly of the microfluidic device. The PDMS cell culture chamber and glass with pores were bonded using a plasma bonder (Harrick Plasma, NY, USA).

FUS System

The FUS system is composed of an arbitrary waveform generator, a radiofrequency power amplifier and the FUS transducer with its impedance matching network. In particular, a 20 MHz arbitrary waveform generator, which is built in a computer-based oscilloscope, (Picoscope 5242B, Pico Technology, Eaton Socon, UK) was connected to a mobile workstation (ThinkPad W540 Mobile Workstation, Lenovo, Morrisville, North Carolina, USA), via a USB 2.0 connection, and was used to generate a sinusoidal signal. This signal was amplified by 50 dB using a 40-W radiofrequency power amplifier (240L, E&I, Rochester, NY, USA) before being fed to the electrical impedance matching network (50 Ohms) of the FUS transducer (built in house). The FUS transducer is a spherically-focused, single-element PZT, with a 30 mm radius of curvature and an F-number of 0.75.

The profile of the focal region of this transducer was characterized by two methods at its operational frequencies: 1.025 MHz and 3.525 MHz. First, a calibrated hydrophone (ONDA, HNC-0200, Sunnyvale, CA, USA) that was attached to a fully automatic 3D positioning system (Velmex Bloomfield, NY, USA) was used to scan the FUS focal region and determine the pressure profile in the axial and transverse directions in the water. Second, a thermochromic film with 2°C bandwidth (35.5 – 37.5 °C) was placed in the focal region and

in direct contact with the microfluidic device to provide a direct visualization of the heated region (i.e. drug-release region). These temperature maps were recorded using a portable digital camera and were analyzed to extract the 2D profile of the heated region (Figure S2, Movie S1 and suppl. methods).

Closed-loop Controller

The closed-loop controller of the FUS system (Figure 2C) includes i) temperature and pressure sensors, ii) a data acquisition system and iii) a computer-based controller that was implemented in MATLAB (MATLAB R2014b, The MathWorks, Natick, MA, USA). We used a T-type thermocouple (built in house) composed of two 20 μm thick constantan and copper insulated wires (California Fine Wires, Grover Beach, CA, USA) that were connected at theirs tips. The pressure sensor was made of a 110 μm thick metalized polyvinylidene difluoride (PVDF) membrane (Measurement Specialities Inc, Hampton, VA, USA) that was etched in-house and connected to a coaxial cable using a high conductivity silver conductive epoxy (EP110, EPO-TEK, Billerica, MA, USA). Both sensors were attached to an acoustically and optically transparent, 100 μm thick, mylar membrane and placed in contact with the glass side of the microfluidic device (Figure 1C). The thermocouple reader (PicoLogger TC-08, Pico Technology, Eaton Socon, UK) and the computer-based oscilloscope were controlled by a MATLAB script that was also used to analyze and display the collected data in real time.

To perform FUS-triggered mild hyperthermia into the device we implemented a binary ON/OFF controller. We set the controller reference temperature to 43.5°C and the FUS transducer to be continuously emitting US waves (ON) for as long as the measured temperature was below the reference temperature. The FUS transducer was switched to standby mode (OFF) when the measured temperature exceeded the reference threshold. The temperature was measured every 0.5 sec. To detect microbubble emissions, ultrasound microbubble contrast agents (Definity, Lantheus Medical Imaging, Billerica, MA, USA) were loaded in the DST flow microchannel and after delivering a 10 msec ultrasound pulse (300 kPa peak negative pressure) the microbubble acoustic emissions were recorded by the PVDF membrane that was operated in passive mode. The measured acoustic emissions were filtered, amplified and digitized by the computer-based oscilloscope, before transferring to the portable workstation for fast fourier transform processing and storage. Strong harmonic, ultra-harmonic or broadband signals (excitation frequency: 1.025 MHz), in the power spectra of the recorded acoustic emissions were used to identify nonlinear microbubble oscillations in the flow microchannel.

Cell Culture and Chemotherapy Response

The F98 rat glioblastoma cell line (ATCC, Manassas, VA, USA) was infected with an in-lab modified pMSCV (Clontech, Mountain View, CA, USA) vector to stably express green fluorescence protein (GFP) in order to monitor tumor cell proliferation in real time. Cells were cultured in RPMI medium supplemented with 10% heat inactivated fetal bovine serum and 1% penicillin/streptomycin (Invitrogen, Grand Island, NY, USA) and grown until 60% confluence. We used a doxorubicin encapsulated temperature-sensitive liposome formulation

(doxorubicin-TS-liposomes) (ThermoDox, Celsion Co, NJ, USA) in combination with mild hyperthermia produced by the FUS system or a water bath to trigger drug release.

Cancer cell drug-response in well plates

Five hundred glioblastoma cells were seeded per well in a 96-well plate and were allowed to grow overnight. Cells were dosed with varying concentrations of doxorubicin-TS-liposomes (Figure 3A) and doxorubicin release was triggered by water bath heating. Cells were incubated with the doxorubicin-TS-liposomes at 37 °C (no drug release conditions) for 12 min or heated at 43 °C (drug release conditions) in a water bath for 12 min [37, 43] to trigger maximum release, followed by a 50 min incubation period to allow for drug diffusion and cell uptake. Next, the wells were washed with fresh medium and 48 hrs later the number of total and dead cells (stained with 1 μM Ethidium Bromide (Sigma, MO, USA)) was measured using an Acumen cytometer (TTP Labtech, Melbourne, UK). Viable cells were calculated by subtracting the number of dead cells from the total number of cells.

Microfluidic experiments

The glioblastoma cells were seeded at a density of 0.1 million cells/mL in a 2 mg/ml type I collagen gel (BD Biosciences, NJ, USA) as described previously [45] and cells were allowed to grow for 48 hrs prior to applying the experimental conditions. 40 μl of doxorubicin-TS-liposome solution was loaded in the inlet port of the DST channel. A stable concentration was achieved in the cell culture chamber within 10 min (Figure S2E and Movie S2). Drug-release was facilitated either by a 12 min heating period via a 43°C water bath or via FUS-triggered heating. This temperature is significantly lower than the threshold of 63°C where collagen fibril denaturation occurs [46]. We allowed the released doxorubicin to diffuse in the cell culture chamber for 50 min (time-scale selected based on previous studies on doxorubicin uptake dynamics[47]) prior to washing the devices twice with fresh medium (see Figure S7 for schematic illustrating protocol). Confocal imaging was performed immediately after treatment (t=0 hrs) and 48 hrs later to measure total and dead cell numbers. For the localized FUS-triggered release experiments (Figure 5), we used a previously published method[47] to quantify doxorubicin uptake (see suppl. Methods and Figure S8).

Cell Imaging and Immunofluorescence Staining

We acquired confocal image stacks with a Nikon A1R laser scanning microscope and a 10X (NA=0.45) objective to characterize fluorescent tracer distribution and to measure tumor cell response to doxorubicin-TS-liposomes in the microfluidic device. The confocal stacks for cell growth and viability included a 3×10 image field montage scan to capture the whole area of the device at three different z-levels (step: 30 μm), while the transport experiments included live imaging (time-step 10 sec) at a single location.

To visualize doxorubicin-induced DNA damage in the glioblastoma cells, the devices were fixed with 4% paraformaldehyde and stained for DAPI (Invitrogen) and rabbit anti-human H2AX (Cell Signaling #2577, MA, USA) detected with a secondary Alexa594 anti-rabbit antibody (Invitrogen). Devices were fixed 4 hrs after experimental treatment to capture the early phase of DNA damage [36]. We used a 20X (NA=0.75) objective to acquire confocal

image stacks for at least 5 regions per device. The expression of H2AX was quantified using ImageJ by analyzing the fluorescent intensity in the cell nucleus for at least 40 glioblastoma cells per condition.

Computational and Experimental Characterization of Drug Transport

A 2D finite element model was developed in COMSOL (4.2 Version, Burlington, MA, USA) to perform time-dependent simulations of drug diffusion in the cell chamber and interpret the FUS-triggered drug release studies. An initial condition of C_0=1 was defined at the region of drug release that was determined by the temperature measurement using the thermochromic film (Figure S2C). Complete doxorubicin release from the liposomes was modeled for every location in the region with a temperature above 41°C. Constant concentration boundary conditions (C_{SINK}=0) were defined at edges of the microfluidic channels and at the gel filling port. Based on previous experimental characterization in 2 mg/ml collagen type I gels [21] we defined a diffusion coefficient of $D=2.5\times10^{-10}$ m^2/s to model diffusion of free doxorubicin after heat-induced release from the liposomes. The numerical grid for performing the simulations consisted of approximately 22000 finite elements. The experimental characterization in the device included measurement of fluorescent intensity profiles of 400 Da (Fluorescein, Invitrogen) and 2 MDa (Texas Red Dextran, Invitrogen) (Figure S2E) tracers that mimic the distribution of the free doxorubicin (MW ~ 535 Da) and doxorubicin-TS-liposomes (~90 nm [48]). The raw intensity fluorescence images were analyzed in MATLAB to compute the average intensity over time and to visualize concentration distributions (Figure 2G, H).

Quantification of Cell Response and Data Analysis

Cell viability and growth in the microfluidic devices under different experimental conditions were measured by quantifying the number of GFP (viable cells) and RFP (dead cells) fluorescence using a custom code in MATLAB. A proliferation metric was computed as the ratio of viable cells at 48 hrs to viable cells at 0 hrs, while the cell death metric was computed as the ratio of dead cells to total cells at 48 hrs. These metrics were evaluated as sums across 10 regions per device, encompassing the whole cell chamber area (see suppl. Methods and Figure S9).

All reported metrics in the microfluidic devices were calculated by averaging the mean values of at least three devices, with each device representing one independent experiment. A range of 20000 to 60000 cells were analyzed per device. T-tests (two-sample, $p<0.05$) were performed in Graphpad Prism (v6, La Jolla CA, USA).

Supplementary Material

Refer to Web version on PubMed Central for supplementary material.

Acknowledgments

This work was supported by a NIH/NIBIB grant (#K99 EB016971) to C.D.A and a Department of Defense, BCRP grant (W81XWH-14-1-0222) to I.K.Z. We thank the Nikon Imaging Center at Harvard Medical School for help with light microscopy and the ICCB-Longwood Screening Facility at Harvard Medical School for providing access to the Acumen ex3 instrument for performing the drug dose-response experiments. Parts of the instrumention used

in our system were developed by Naeal Abu Speitan, Carolynn Chang, and Emily Hudson from the Department of Bioengineering, Boston University, as part of their senior design project (DEBUT Challenge 2014). We acknowledge Sebastien Uzel, Suman Bose and Vasileios Askoxylaki for feedback.

References

1. Chauhan VP, Jain RK. Nature materials. 2013; 12(11):958–62. [PubMed: 24150413]
2. Woodworth GF, Dunn GP, Nance EA, Hanes J, Brem H. Frontiers in oncology. 2014; 4:126. [PubMed: 25101239]
3. Olson JJ, Nayak L, Ormond DR, Wen PY, Kalkanis SN, Ryken TC, Committee ACJG. Journal of neuro-oncology. 2014; 118(3):557–99. [PubMed: 24740195]
4. Bertrand N, Wu J, Xu X, Kamaly N, Farokhzad OC. Advanced drug delivery reviews. 2014; 66:2–25. [PubMed: 24270007]
5. Xu X, Ho W, Zhang X, Bertrand N, Farokhzad O. Trends in molecular medicine. 2015; 21(4):223–32. [PubMed: 25656384]
6. Weiser JR, Saltzman WM. Journal of controlled release : official journal of the Controlled Release Society. 2014; 190:664–73. [PubMed: 24801251]
7. Aryal M, Arvanitis CD, Alexander PM, McDannold N. Advanced drug delivery reviews. 2014; 72:94–109. [PubMed: 24462453]
8. Rapoport N, Gao Z, Kennedy A. Journal of the National Cancer Institute. 2007; 99(14):1095–106. [PubMed: 17623798]
9. Ta T, Bartolak-Suki E, Park EJ, Karrobi K, McDannold NJ, Porter TM. Journal of controlled release : official journal of the Controlled Release Society. 2014; 194:71–81. [PubMed: 25151982]
10. Aryal M, Vykhodtseva N, Zhang YZ, Park J, McDannold N. Journal of controlled release : official journal of the Controlled Release Society. 2013; 169(1–2):103–11. [PubMed: 23603615]
11. Staruch RM, Hynynen K, Chopra R. International journal of hyperthermia : the official journal of European Society for Hyperthermic Oncology, North American Hyperthermia Group. 2015; 31(2): 118–33.
12. Lammertink BH, Bos C, Deckers R, Storm G, Moonen CT, Escoffre JM. Frontiers in pharmacology. 2015; 6:138. [PubMed: 26217226]
13. Leong DT, Ng KW. Advanced drug delivery reviews. 2014; 79–80:95–106.
14. Muller PY, Milton MN. Nature reviews Drug discovery. 2012; 11(10):751–61. [PubMed: 22935759]
15. Sackmann EK, Fulton AL, Beebe DJ. Nature. 2014; 507(7491):181–9. [PubMed: 24622198]
16. Shin Y, Han S, Jeon JS, Yamamoto K, Zervantonakis IK, Sudo R, Kamm RD, Chung S. Nature protocols. 2012; 7(7):1247–59. [PubMed: 22678430]
17. Albanese A, Lam AK, Sykes EA, Rocheleau JV, Chan WC. Nature communications. 2013; 4:2718.
18. Wood LB, Ge R, Kamm RD, Asada HH. Integrative biology : quantitative biosciences from nano to macro. 2012; 4(9):1081–9. [PubMed: 22847074]
19. Dura B, Dougan SK, Barisa M, Hoehl MM, Lo CT, Ploegh HL, Voldman J. Nature communications. 2015; 6:5940.
20. Zervantonakis IK, Hughes-Alford SK, Charest JL, Condeelis JS, Gertler FB, Kamm RD. Proceedings of the National Academy of Sciences of the United States of America. 2012; 109(34): 13515–20. [PubMed: 22869695]
21. Funamoto K, Zervantonakis IK, Liu Y, Ochs CJ, Kim C, Kamm RD. Lab on a chip. 2012; 12(22): 4855–63. [PubMed: 23023115]
22. Kwak B, Ozcelikkale A, Shin CS, Park K, Han B. Journal of controlled release : official journal of the Controlled Release Society. 2014; 194:157–67. [PubMed: 25194778]
23. Sung KE, Beebe DJ. Advanced drug delivery reviews. 2014; 79–80:68–78.
24. Bhatia SN, Ingber DE. Nature biotechnology. 2014; 32(8):760–72.
25. Jakobsson O, Grenvall C, Nordin M, Evander M, Laurell T. Lab on a chip. 2014; 14(11):1943–50. [PubMed: 24763517]
26. Marmottant P, Hilgenfeldt S. Nature. 2003; 423(6936):153–6. [PubMed: 12736680]

27. Bazou D, Castro A, Hoyos M. Ultrasonics. 2012; 52(7):842–50. [PubMed: 22534062]
28. Mulvana H, Cochran S, Hill M. Advanced drug delivery reviews. 2013; 65(11–12):1600–10. [PubMed: 23906935]
29. Forslund E, Guldevall K, Olofsson PE, Frisk T, Christakou AE, Wiklund M, Onfelt B. Frontiers in immunology. 2012; 3:300. [PubMed: 23060879]
30. Guo F, Li P, French JB, Mao Z, Zhao H, Li S, Nama N, Fick JR, Benkovic SJ, Huang TJ. Proceedings of the National Academy of Sciences of the United States of America. 2015; 112(1): 43–8. [PubMed: 25535339]
31. Stan AC, Casares S, Radu D, Walter GF, Brumeanu TD. Anticancer research. 1999; 19(2A):941–50. [PubMed: 10368637]
32. Cheng Z, Al Zaki A, Hui JZ, Muzykantov VR, Tsourkas A. Science. 2012; 338(6109):903–10. [PubMed: 23161990]
33. Barth RF, Kaur B. Journal of neuro-oncology. 2009; 94(3):299–312. [PubMed: 19381449]
34. Dewhirst MW, Viglianti BL, Lora-Michiels M, Hanson M, Hoopes PJ. International journal of hyperthermia : the official journal of European Society for Hyperthermic Oncology, North American Hyperthermia Group. 2003; 19(3):267–94.
35. McDannold N, Vykhodtseva N, Jolesz FA, Hynynen K. Magnetic resonance in medicine. 2004; 51(5):913–23. [PubMed: 15122673]
36. Ikeda M, Kurose A, Takatori E, Sugiyama T, Traganos F, Darzynkiewicz Z, Sawai T. International journal of oncology. 2010; 36(5):1081–8. [PubMed: 20372780]
37. Needham D, Anyarambhatla G, Kong G, Dewhirst MW. Cancer research. 2000; 60(5):1197–201. [PubMed: 10728674]
38. De Juan BS, Von Briesen H, Gelperina SE, Kreuter J. Journal of drug targeting. 2006; 14(9):614–22. [PubMed: 17090397]
39. Al-Ahmady ZS, Scudamore CL, Kostarelos K. International journal of cancer Journal international du cancer. 2015; 137(3):731–43. [PubMed: 25639452]
40. ter Haar G. International journal of hyperthermia : the official journal of European Society for Hyperthermic Oncology, North American Hyperthermia Group. 2015; 31(2):75–6.
41. Carugo D, Owen J, Crake C, Lee JY, Stride E. Ultrasound in medicine & biology. 2015; 41(7): 1927–37. [PubMed: 25922133]
42. Arvanitis CD, Bazan-Peregrino M, Rifai B, Seymour LW, Coussios CC. Ultrasound in medicine & biology. 2011; 37(11):1838–52. [PubMed: 21963037]
43. Escoffre JM, Novell A, de Smet M, Bouakaz A. Physics in medicine and biology. 2013; 58(22): 8135–51. [PubMed: 24200816]
44. Gourevich D, Volovick A, Dogadkin O, Wang L, Mulvana H, Medan Y, Melzer A, Cochran S. Ultrasound in medicine & biology. 2015; 41(7):1853–64. [PubMed: 25887690]
45. Shin Y, Han S, Jeon JS, Yamamoto K, Zervantonakis IK, Sudo R, Kamm RD, Chung S. Nature protocols. 2012; 7(7):1247–59. [PubMed: 22678430]
46. Suwa Y, Nam K, Ozeki K, Kimura T, Kishida A, Masuzawa T. Journal of biomedical materials research. Part B, Applied biomaterials. 2015
47. Shen F, Chu S, Bence AK, Bailey B, Xue X, Erickson PA, Montrose MH, Beck WT, Erickson LC. The Journal of pharmacology and experimental therapeutics. 2008; 324(1):95–102. [PubMed: 17947497]
48. Li L, ten Hagen TL, Hossann M, Suss R, van Rhoon GC, Eggermont AM, Haemmerich D, Koning GA. Journal of controlled release : official journal of the Controlled Release Society. 2013; 168(2): 142–50. [PubMed: 23524188]

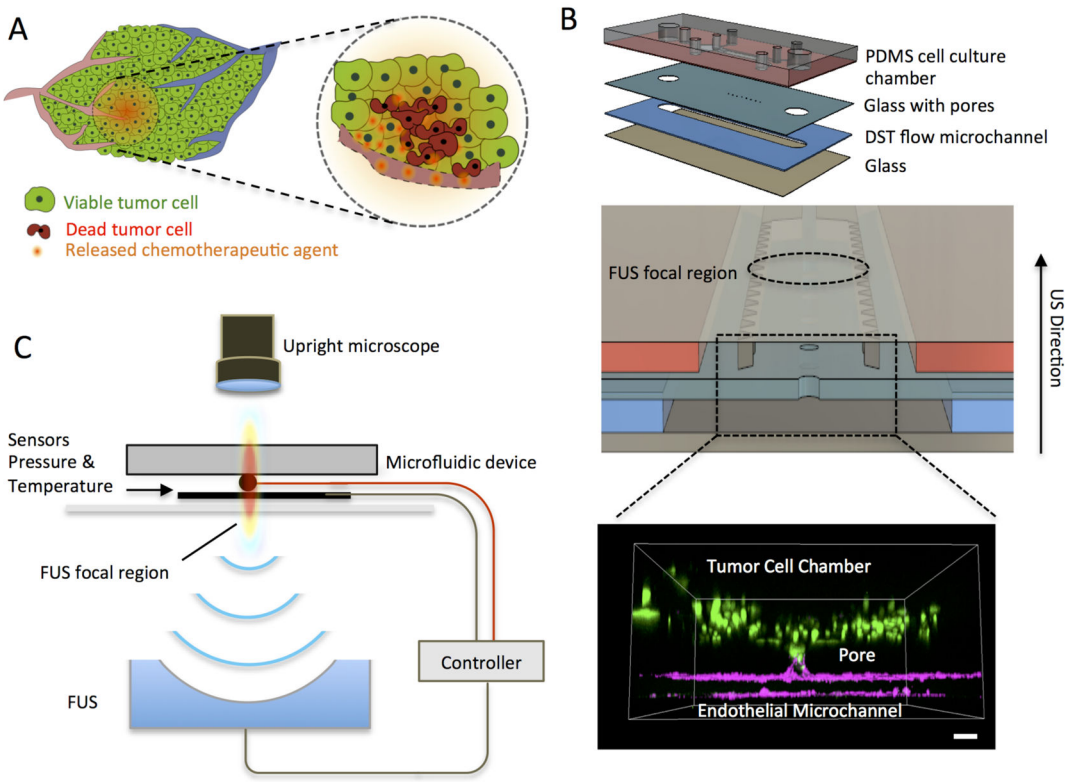

Figure 1.

Schematic of the closed-loop acoustofluidic (FUS-microfluidic integrated) device. (A) Schematic showing localized, drug release in a tumor. The area targeted for drug release by FUS is highlighted with the dashed circle. (B) Top: Assembly of the multilayer microfluidic device. Middle: Cross-section of the microfluidic device showing the cell chamber, DST flow microchannel where the drugs are loaded and the FUS focal region. Bottom: 3D confocal rendering of GFP tumor cells (green) in the cell chamber and interfaced through the glass pore with the DST flow microchannel where an endothelial monolayer is formed (magenta) (C) Diagram of experimental system, highlighting the optically transparent microfluidic device, the pressure/temperature sensors feeding into the controller and the FUS transducer (located 30mm away from the device).

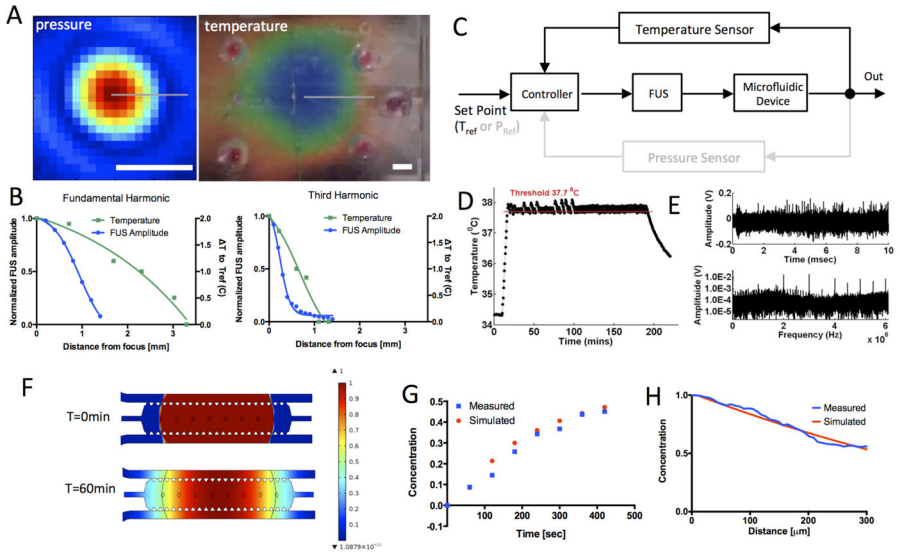

Figure 2.

Computational and experimental characterization of the acoustofluidic system. (A) Pressure (left) and temperature (right) maps for the fundamental frequency (1.025MHz) of the FUS transducer. Pressure map was measured with a calibrated hydrophone in the water. The temperature was mapped using a thermochromic film with 2 °C dynamic range. Scalebar is 2mm. (B) Spatial profiles of FUS amplitude (blue) and temperature (green) for the fundamental (left) and third harmonic (right). FUS amplitude was normalized by the maximum value. (C) Controller block diagram. (D) Temperature recording from the thermocouple in response to FUS pulses. Feedback control was used for all temperature measurements in our experiments. (E) Voltage trace (top) and spectrum (bottom) of microbubble acoustic emissions recorded by the pressure sensor in response to a FUS pulse. Temperature and pressure sensors are located in the center of the heated region in Figure 2A. (F) Simulations of concentration distribution of the released drug at time 0 (top) and 60min (bottom). (G) Measured and computed temporal evolution of drug concentration 100μm from the initial drug-release area. (H) Concentration profiles within the cell chamber at t=60min. Concentration values were normalized by the maximum value in the drug-release area.

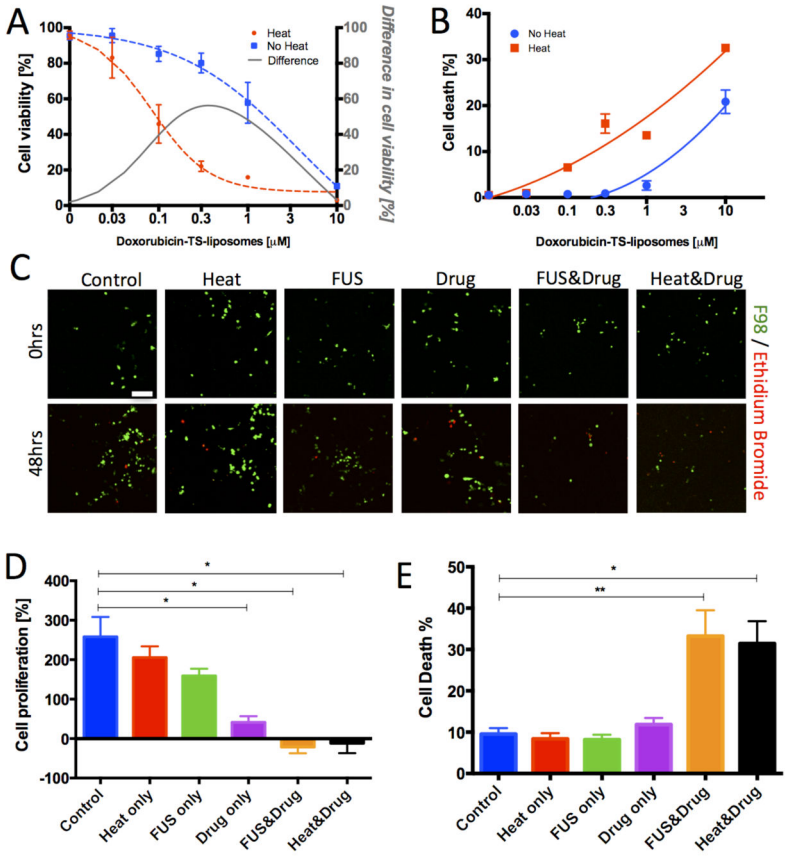

Figure 3.

Cancer cell response to doxorubicin-TS-liposomes. (A) F98 cell viability to varying drug doses after 48hrs under water-bath triggered release (red) and no-release (blue) conditions. Viability values normalized to the untreated control. The difference between the two curves is also plotted (grey). (B) Cell death dose-response (a quadratic function was fit). Average values and SEM error bars across 4 wells. (C) Top: Representative confocal images of viable (green) and dead (red) F98 cells in the microfluidic device prior (top: 0hrs) and after (bottom: 48hrs) application of experimental conditions. Each image corresponds to a single confocal slice. Scale bar is 100μm. (D) Quantification of cell proliferation (% change of viable cells between 48hrs and 0hrs) in the microfluidic device under control, heating only, FUS treatment only, doxorubicin-TS-liposomes (0.3 μM) only, FUS & doxorubicin-TS-liposomes (0.3 μM), water-bath induced-heating at 43C & doxorubicin-TS-liposomes (0.3 μM). (E): Percentage of dead cells over total cells in each condition. Average values across n > 5 devices; error bars represent standard error of the mean (SEM). Statistically significant differences are highlighted (* $p<0.05$; ** $p<0.01$).

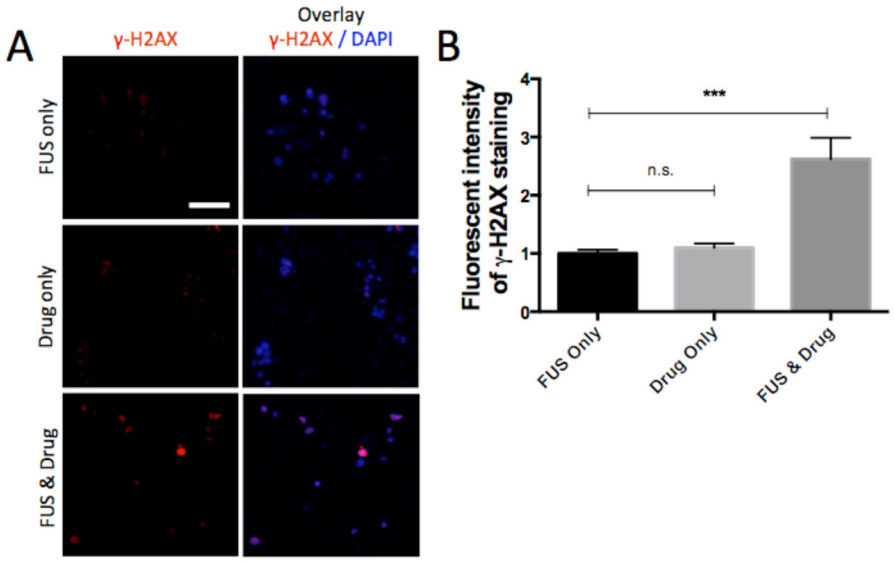

Figure 4.

Analysis of DNA damage in response to drug exposure in the device. (A) Immunostaining of γ-H2AX and DAPI in the microfluidic device under conditions of FUS-exposure, no-drug release (0.3μM doxorubicin-TS-liposomes) and FUS-triggered drug release (FUS & drug: 0.3μM). Each image corresponds to a single confocal slice. Scale bar corresponds to 100μm. (B) Quantification of staining intensity per cell in (A). Average values (n=40), and error bars represent standard deviation. Values normalized to the γ-H2AX intensity for the FUS only condition. Statistically significant differences are highlighted (*** $p<0.001$).

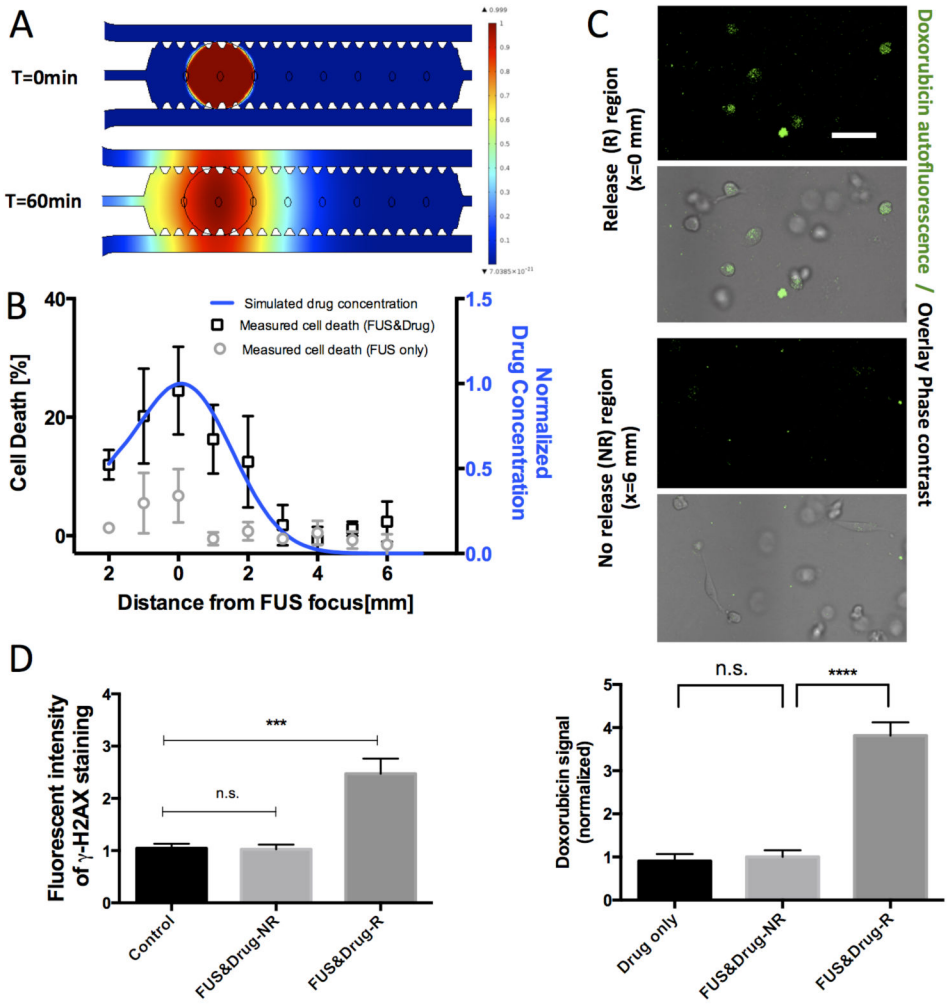

Figure 5.

Localized FUS-triggered drug release and cell response. (A) Diffusion simulation of drug distribution at 0min and 60min after FUS-triggered release. (B) Spatial profile (blue) of simulated drug concentration at t=60minutes after drug release and measured cell death under localized FUS-triggered drug treatment (black bars) show good agreement. Cell death profile under FUS-treatment only (grey bars) is also shown. Concentration normalized to the maximum value (0.3μM). Cell death values are reported as differences from baseline values at the region of no release. Averages across n=4 devices and error bars are SEM. (C) Representative confocal images of doxorubicin uptake (green) in an area of drug release (R) compared to an area of no release (NR), 1hr after FUS-triggered heating. Scale bar corresponds to 50μm. Quantification of doxorubicin (dose of 3μM to clearly demonstrate differential effects) uptake in microfluidic devices. Values are normalized to doxorubicin uptake signal for devices treated with drug only but no FUS treatment. Average values across n=30 cells are plotted, and error bars represent standard deviation. (D) Quantification of DNA-damage response in drug release (R) and no release (NR) locations in devices 4hrs after localized FUS treatment and doxorubicin-TS-liposome (0.3μM) treatment. Bars represent average across n=40 cells, and error bars represent standard deviation. Values

normalized to the γ-H2AX intensity for the untreated control. Statistically significant differences are highlighted (*** $p<0.001$, **** $p<0.0001$).

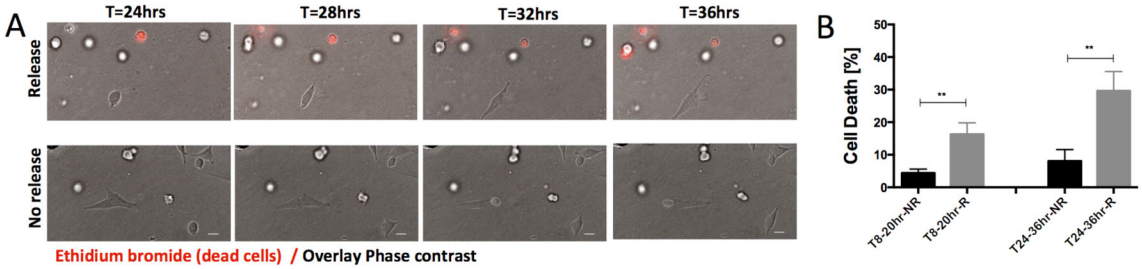

Figure 6.

Live cell imaging of tumor cell death after FUS-triggered localized drug release. (A) Time series of confocal images showing tumor cell death (red, incorporation of ethidium bromide) in a location of drug release (top row) compared to a location of no release (bottom row). Scale bar corresponds to 25μm. (B) Quantification of the percentage of tumor cells dying during 8–20hrs (left) and 24–36hrs (right) after treatment with doxorubicin-TS-liposomes (3μM) in areas of drug release (R) and areas of no release (NR). n=8 locations were analyzed per condition (n>120 cells scored per condiction per device) and values represents averages with error bars SEM. Statistically significant differences are highlighted (** $p<0.01$).